INTERNATIONAL JOURNAL FOR NUMERICAL METHODS IN FLUIDS, VOL. 12, 765–783 (1991)

RADIATION BOUNDARY CONDITIONS FOR FINITE ELEMENT SOLUTIONS OF GENERALIZED WAVE EQUATIONS

MATTHIAS JOHNSEN

Thayer School of Engineering, Dartmouth College, Hanover, NH 03755, U.S.A., and Aerodynamisches Institut, RWTH Aachen, Templergraben 55, D-5100 Aachen, Federal Republic of Germany

KEITH D. PAULSEN

Thayer School of Engineering, Dartmouth College, Hanover, NH 03755, U.S.A.

AND

FRANCISCO E. WERNER

Skidaway Institute of Oceanography, PO Box 13687, Savannah, GA 31416, U.S.A.

SUMMARY

On the basis of the dispersion relation of the generalized linear wave equation we derive a radiation boundary condition (RBC) that explicitly incorporates the physical parameters of the governing equation into the form of the boundary condition. Using finite element techniques we investigate the properties of the generalized RBC by examining forced and unforced solutions to the telegraph and Klein–Gordon equations in one dimension. The results show that within the limits of the physical parameters of the problem the generalized RBC is an improvement over the Sommerfeld RBC when the governing equation contains additional terms that influence the propagation. These gains are achieved without introducing any computational overhead. A two-dimensional example suggests that the 1D findings can generalize to higher dimensions.

KEY WORDS Radiation boundary conditions Open boundary conditions Wave equation Finite elements

INTRODUCTION

The need to apply radiation boundary conditions (RBCs) occurs when waves or propagating signals reach the open boundaries of a computational domain. At such boundaries the outward (inward) travelling waves must be allowed to exit (enter) the domain without artificial wave reflection or trapping. In finite difference and finite element solutions of unbounded wave propagation problems, open boundaries arise as non-physical features resulting from mesh truncation. Although a variety of open boundary conditions have been studied (e.g. References 1–3), Sommerfeld conditions are perhaps the most widely used. The study of Sommerfeld RBCs[4] has been an active research area and various forms have been investigated (e.g. References 5–15).

The form of the Sommerfeld condition commonly implemented at the open boundary,

$$\frac{\partial \zeta}{\partial t} \pm c \frac{\partial \zeta}{\partial n} = 0, \tag{1a}$$

0271–2091/91/080765–19$09.50

Received 12 September 1989
Revised 15 May 1990

is an approximation of the general condition of radiation derived by Sommerfeld for the wave equation

$$\frac{\partial^2 \zeta}{\partial t^2} - c^2 \nabla^2 \zeta = \rho, \tag{1b}$$

where ζ is the physical quantity of interest, ρ is a source term, c is the phase speed, t is time, ∇^2 is the Laplacian operator and $\partial/\partial n$ is the derivative normal to the boundary. Condition (1a) is exact when applied analytically or at infinity. It is only approximately correct when numerical discretization errors occur at a finite boundary or when the 1D condition is used in higher-dimensional problems. The approximation results in reflections that become more severe as the obliqueness of the angle of incidence of the impinging waves increases, as is the case when the location of the open boundary is near the source of the propagating waves. Although in certain applications exact formulations of open boundary conditions are available (e.g. References 16–18), the localized (and partially reflecting) RBCs have generally been favoured due to the ease in their implementation and their computational economies. Higher-order approximations that have succeeded in reducing reflections from the numerical boundaries include References 6, 19 and 20.

It is safe to say that when a motion of interest is governed by the wave equation in the vicinity of the open boundary—either because the problem does not contain additional physical processes or because the open boundary has been placed far from the regions where sources are significant—a variety of adequate Sommerfeld-based RBCs are available. However, many problems are governed by more generalized wave equations which contain additional terms such as dissipation. Hence it is reasonable to expect that since the form of the governing equation has been altered to accommodate additional effects in these cases, so too must the form of the RBC.

To illustrate this point, consider the simple 1D problem of a freely propagating disturbance of prescribed initial shape in a dissipative medium governed by the telegraph equation

$$\frac{\partial^2 \zeta}{\partial t^2} + \tau \frac{\partial \zeta}{\partial t} - c^2 \nabla^2 \zeta = 0, \tag{2}$$

where τ is a dissipation or loss factor ($\tau > 0$). Numerical results for the freely propagating disturbance are shown in Figure 1 for the solution to (2) subject to the Sommerfeld RBC (1a) and an extended grid solution which is free of boundary effects.

The telegraph equation, which contains the additional dissipative term, behaves differently from its pure wave equation counterpart. The inclusion of dissipation alters the solution, combining the results of the wave equation and a diffusion equation: there is a propagating component and a component which decays on a diffusive timescale dependent on τ. As shown in Figure 1, the Sommerfeld RBC is inadequate at the open boundary in the presence of dissipation. The Sommerfeld RBC produces a spurious steady state value which is absent from the extended grid solution.

Another example is shown in Figure 2 where a one-dimensional form of the Klein–Gordon equation is solved subject to the Sommerfeld RBC. The Klein–Gordon equation can be written as

$$\frac{\partial^2 \zeta}{\partial t^2} - c^2 \nabla^2 \zeta + c^2 \mu^2 \zeta = 0, \tag{3}$$

where μ is an elasticity factor ($\mu > 0$). Here a continual sinusoidal forcing has been applied and results are plotted for the dynamic steady state. The motion may be thought of as that of a flexible string embedded in a rubber sheath which adds a restoring force on each portion of the string (Reference 21, pp. 138–141). For the forced case the propagation is similar to that of the pure wave

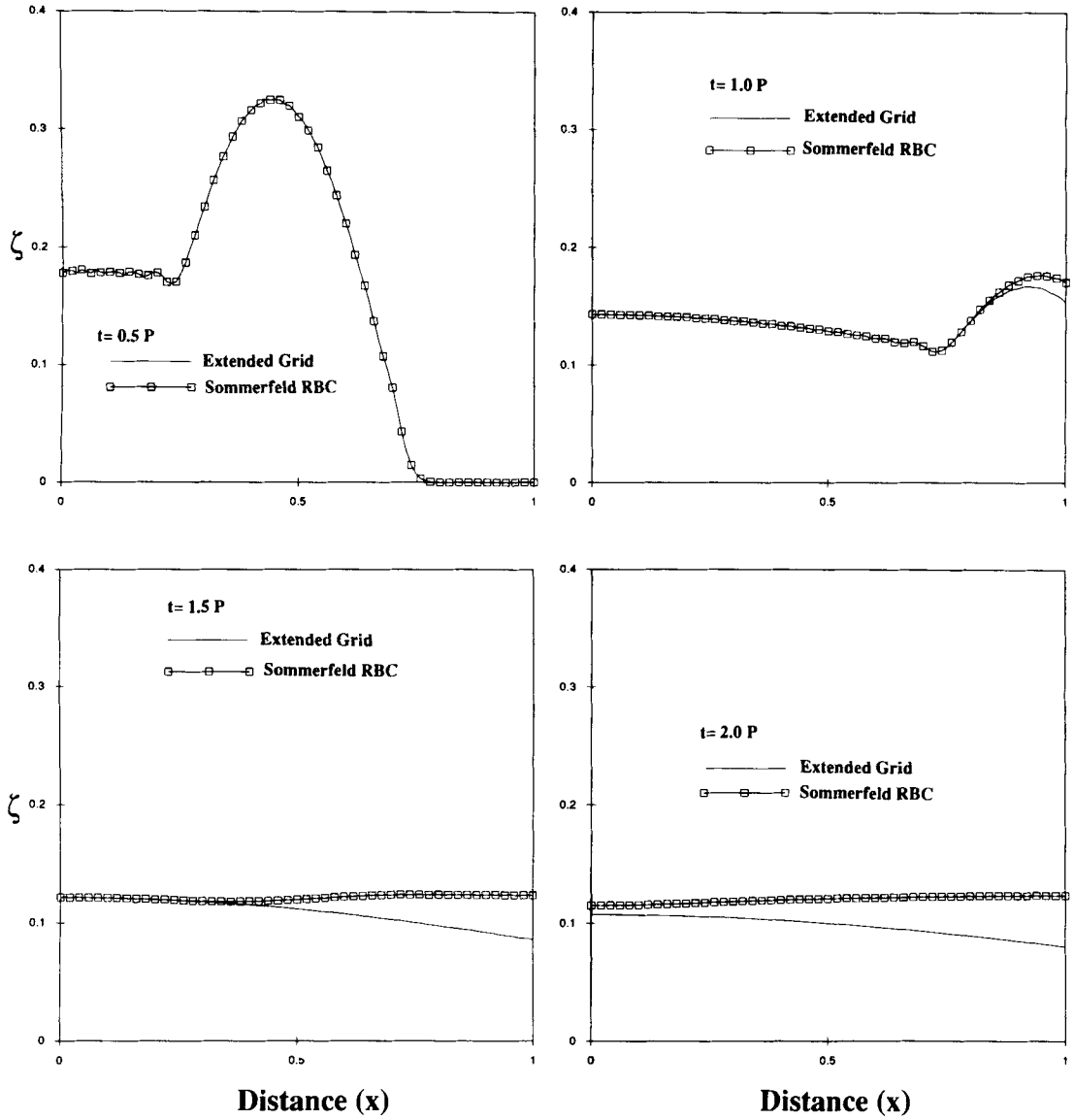

Figure 1. A time sequence of telegraph equation propagation of an initial disturbance subject to the Sommerfeld RBC. The open boundary is located at the right edge of each plot. The length of the grid is λ, $\tau/\omega = 0{\cdot}5$ and the time instants occur 0·5, 1·0, 1·5 and 2·0 periods into the simulation. See text for further details

equation except that the additional elastic forces act to increase the wave speed. Figure 2 shows that the Sommerfeld RBC does not behave as a transparent boundary for this wave motion either.

The inadequacy of the Sommerfeld condition as an RBC for the governing equations describing the motion in Figures 1 and 2 suggests that alternative RBCs are needed for cases where the wave equation has a more general form over the entire region of interest *including* the neighbourhood of the open boundary. This feature has been recognized previously and various schemes have been

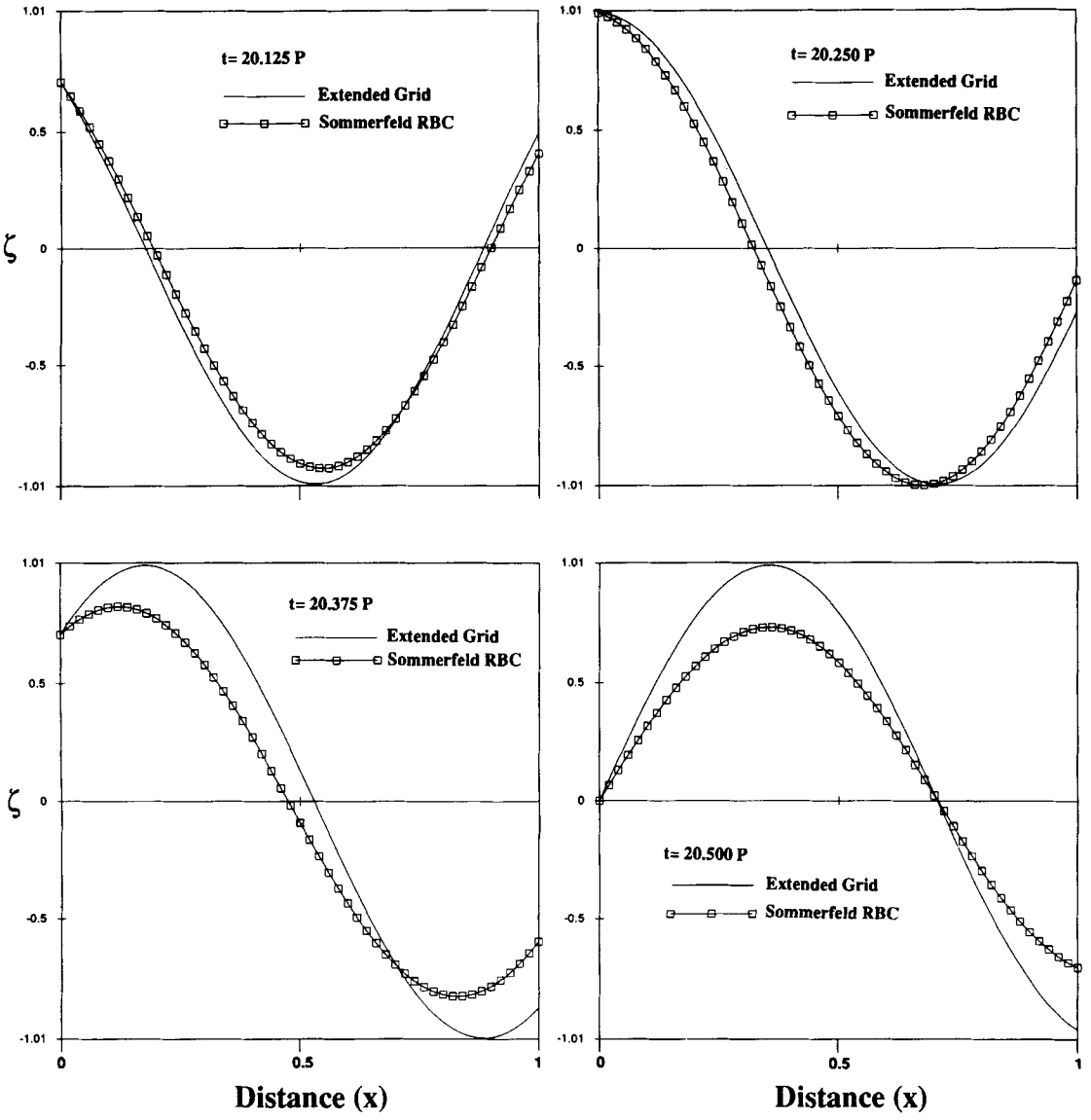

Figure 2. A time sequence of a sinusoidally forced Klein–Gordon equation solution subject to the Sommerfeld RBC. The open boundary is located at the right edge of each plot. The length of the grid is λ, $c^2\mu^2/\omega^2 = 0{\cdot}50$ and the time instants occur 20·125, 20·25, 20·375 and 20·5 periods into the simulation. See text for further details

developed to account for the added effects near the boundaries. One of these is discussed in Reference 5 wherein the Sommerfeld condition is used, but rather than fixing the phase speed as a constant, it is numerically calculated from neighbouring grid points.

The approach we take herein, rather than relying on the computation of the phase speed during the simulation, takes advantage of the *a priori* knowledge of the form of the governing equation to construct an RBC which will be consistent (although approximate) with the physics of the problem. We derive and study boundary conditions by examining the dispersion relationship for

the full equation, not just the wave equation limit. As a result, other terms will arise in the RBC which *explicitly* include the effects of additional factors in the governing equation.

In the next section the derivation of a generalized RBC is given. This is followed by a description of the implementation of such a condition in the context of finite elements. Specific RBCs are then studied for the telegraph and Klein–Gordon equations. Their behaviour in both forced and unforced cases is examined relative to the solution computed on an extended grid where the boundary effects are absent. We focus on 1D results in order to investigate the simplest situations; a 2D extension is presented at the end of the paper for illustration purposes.

THE GENERALIZED RADIATION BOUNDARY CONDITION

Consider the linear 1D wave equation of the form

$$\frac{\partial^2\zeta}{\partial t^2}-c^2\frac{\partial^2\zeta}{\partial x^2}+c_1\zeta+c_2\frac{\partial\zeta}{\partial x}+c_3\frac{\partial\zeta}{\partial t}+c_4\frac{\partial^2\zeta}{\partial t\,\partial x}=0. \tag{4}$$

We will construct a generalized RBC by studying an approximate form for the dispersion relationship of (4), identifying a partial differential equation (PDE) for which the approximation is the exact dispersion relation, and use this PDE as an enforceable boundary condition.

Assume a plane wave solution of the form

$$\zeta=\zeta_0 e^{j(-\omega t+\kappa x)}, \tag{5}$$

where $j=\sqrt{(-1)}$, κ is the wavenumber, ζ_0 is the amplitude and ω is the angular frequency. Substituting (5) into (4) results in the dispersion relation

$$\omega^2-c^2\kappa^2-c_1-jc_2\kappa+jc_3\omega-c_4\kappa\omega=0, \tag{6}$$

which is rewritten as

$$\kappa=\pm\frac{\omega}{c}\sqrt{\left(1-\frac{c_1}{\omega^2}-j\frac{c_2\kappa}{\omega^2}+j\frac{c_3}{\omega}-\frac{c_4\kappa}{\omega}\right)}. \tag{7}$$

Note that we have not solved for κ; we have only rearranged (6). Following Trefethen and Halpern,[20] equation (7) is linearized according to

$$\sqrt{(1+\chi)}\approx 1+\chi/2, \tag{8}$$

where χ ($|\chi|<1$) represents the collection of terms with coefficients $c_1 \ldots c_4$ from (7). Using the approximation of (8) in equation (7) yields

$$\mp c\omega\kappa+\omega^2-\frac{c_1}{2}-j\frac{c_2\kappa}{2}+j\frac{c_3\omega}{2}-\frac{c_4\kappa\omega}{2}=0, \tag{9}$$

which can be identified as the dispersion relation of the PDE

$$\frac{\partial^2\zeta}{\partial t^2}+\left(\frac{c_4}{2}\pm c\right)\frac{\partial^2\zeta}{\partial x\,\partial t}+\frac{c_1}{2}\zeta+\frac{c_2}{2}\frac{\partial\zeta}{\partial x}+\frac{c_3}{2}\frac{\partial\zeta}{\partial t}=0. \tag{10}$$

Equation (10) becomes the proposed radiation boundary condition for the generalized wave equation (4). The requirement that $|\chi|<1$ in (8) for the derivation of (10) implies that the problem should be largely governed by the wave equation, with other effects or terms having a smaller effect on the motion. This approximation will, of course, be more accurate the more 'plane-wave-like' the propagation is at the boundary and the more closely an equality in (8) can be achieved.

For the telegraph and Klein–Gordon equations (2) and (3), the proposed RBCs for outward-travelling waves become

$$\frac{\partial^2\zeta}{\partial t^2}+c\frac{\partial^2\zeta}{\partial t\partial x}+\frac{\tau}{2}\frac{\partial\zeta}{\partial t}=0 \tag{11}$$

and

$$\frac{\partial^2\zeta}{\partial t^2}+c\frac{\partial^2\zeta}{\partial t\partial x}+\frac{c^2\mu^2}{2}\zeta=0 \tag{12}$$

respectively.

FINITE ELEMENT IMPLEMENTATION

In this section we detail the numerical (finite element) formulation for the telegraph equation and associated RBC (11). Implementation of the Klein–Gordon equation and its RBC (12) as well as other variants of (4) and (10) proceeds in a similar manner. We will be explicit wherever details for the implementation of the Klein–Gordon equation differ significantly from the telegraph equation.

The weighted residual statement of equation (2) is

$$\left\langle\frac{\partial^2\zeta}{\partial t^2},\phi_i\right\rangle+\left\langle\tau\frac{\partial\zeta}{\partial t},\phi_i\right\rangle-\langle c^2\nabla^2\zeta,\phi_i\rangle=0, \tag{13}$$

where ϕ_i is a scalar weighting function and the notation $\langle a, b\rangle$ is the inner product operator (the integral over the domain of interest of the product of a and b). The weak form of (13) is

$$\left\langle\frac{\partial^2\zeta}{\partial t^2},\phi_i\right\rangle+\left\langle\tau\frac{\partial\zeta}{\partial t},\phi_i\right\rangle+\langle c^2\nabla\zeta,\nabla\phi_i\rangle=+\oint c^2\nabla\zeta\cdot\hat{\mathbf{n}}\phi_i\,\mathrm{d}s, \tag{14}$$

where the surface integral includes the open boundary and $\hat{\mathbf{n}}$ is the unit outward-pointing normal. The 1D form of (14) is

$$\left\langle\frac{\partial^2\zeta}{\partial t^2},\phi_i\right\rangle+\left\langle\tau\frac{\partial\zeta}{\partial t},\phi_i\right\rangle+\left\langle c^2\frac{\partial\zeta}{\partial x},\frac{\partial\phi_i}{\partial x}\right\rangle=+c^2\frac{\partial\zeta}{\partial x}\phi_i\Big|_{x=-L}^{x=+L}, \tag{15}$$

where the right-hand-side term is evaluated at the open boundaries located at $x=\pm L$.

The Bubnov–Galerkin variant of the method of weighted residuals is employed such that the basis functions ϕ_j used in the approximation of the unknown

$$\zeta\approx\sum\zeta_j\phi_j \tag{16}$$

are identical to the weighting functions used in (13)–(15). In the calculations that follow, piecewise linear basis functions are implemented (1D chapeau functions or 2D linear triangular elements). The domain integrations are computed by placing the quadrature points coincident with the element nodes.[22] With this nodal quadrature rule, a centred (three-level) finite difference treatment of the time derivatives results in a fully explicit scheme in time.

The difference expressions used for the time derivatives are

$$\frac{\partial\zeta}{\partial t}=\frac{\zeta^{k+1}-\zeta^{k-1}}{2\Delta t}=\frac{\Delta\zeta}{2\Delta t}, \tag{17a}$$

$$\frac{\partial^2\zeta}{\partial t^2}=\frac{\Delta\zeta-2(\zeta^k-\zeta^{k-1})}{\Delta t^2}, \tag{17b}$$

where k indicates the time level, Δt is the time step size and $\Delta\zeta \equiv \zeta^{k+1} - \zeta^{k-1}$. Substituting these expressions into (14) and using (16) yields

$$S_{ij}\Delta\zeta_j = P_{ij}(\zeta_j^k - \zeta_j^{k-1}) - \Delta t^2 Q_{ij}\zeta_j^k + \Delta t^2 c^2 \oint \frac{\partial \zeta}{\partial n}\phi_i \, \mathrm{d}s, \tag{18}$$

where $S_{ij} = \langle (1 + \tau\Delta t/2)\phi_i\phi_j \rangle$, $P_{ij} = \langle 2\phi_i\phi_j \rangle$ and $Q_{ij} = \langle c^2 \nabla\phi_i \cdot \nabla\phi_j \rangle$. Using the nodal quadrature rule for the spatial integrations, S_{ij} collapses to a diagonal matrix S_i with no matrix inversion required. Hence (18) produces an explicit expression for nodal values of ζ at time $k+1$ in terms of known values at k and $k-1$.

The RBC is introduced into the term on the right-hand side of (14). An explicit form of the boundary condition equation is enforced by making use of (17a,b) and solving for $\partial\zeta/\partial n$. For simplicity, consider the 1D case, equation (15). Time integration of (11) results in

$$\frac{\partial \zeta}{\partial t} + c\frac{\partial \zeta}{\partial x} + \frac{\tau}{2}\zeta = 0, \tag{19}$$

which is solved for ζ_x^* and substituted into the right-hand side of (15) such that

$$+c^2 \frac{\partial \zeta}{\partial x}\phi_j \Big|_{x=-L}^{x=+L} = -c\left(\frac{\Delta\zeta}{2\Delta t} + \frac{\tau}{2}\zeta^k\right)\Big|_{x=+L} - c\left(\frac{\Delta\zeta}{2\Delta t} + \frac{\tau}{2}\zeta^k\right)\Big|_{x=-L} \tag{20}$$

In 2D the evaluation of the boundary integral at boundary node B leads to

$$+\oint \frac{\partial \zeta}{\partial n}\phi_j \, \mathrm{d}s = -\frac{1}{c}\left(\frac{\zeta_B^{k+1} - \zeta_B^{k-1}}{2\Delta t} + \frac{\tau}{2}\zeta_B^k\right)\oint \phi_B \, \mathrm{d}s = -\frac{1}{c}\left(\frac{\zeta_B^{k+1} - \zeta_B^{k-1}}{2\Delta t} + \frac{\tau}{2}\zeta_B^k\right)\left(\frac{\Delta b_1 + \Delta b_2}{2}\right), \tag{21}$$

where Δb_1 and Δb_2 are the lengths of the boundary segments adjacent to the node of interest. For equally spaced nodes (with a node spacing δ), the right side of (14) can be simplified to

$$+c^2 \oint \nabla\zeta \cdot \hat{\mathbf{n}}\phi_j \, \mathrm{d}s \approx -\frac{c\delta}{2}\left(\frac{\zeta_B^{k+1} - \zeta_B^{k-1}}{\Delta t} + \tau\zeta_B^k\right) \tag{22}$$

for each of the B boundary node equations.

Implementation of RBC (12) for the Klein–Gordon equation proceeds similarly except that the second-order time derivative cannot be removed and must be dealt with explicitly. An explicit form of boundary condition equation (12) can be written as

$$\frac{\Delta\zeta - 2(\zeta^k - \zeta^{k-1})}{\Delta t^2} + c\left(\frac{\zeta_x^{k+1} - \zeta_x^{k-1}}{2\Delta t}\right) + \frac{c^2\mu^2}{2}\zeta^k = 0. \tag{23}$$

Solving (23) for ζ_x at the new time level produces

$$+c^2\zeta_x^{k+1} = -c\left(\frac{2\Delta\zeta - 4(\zeta^k - \zeta^{k-1})}{\Delta t}\right) - \Delta t c^3\mu^2\zeta^k + c^2\zeta_x^{k-1}, \tag{24}$$

which can be substituted into the right side of (15) to close the algebraic system since it consists only of the unknown boundary value of ζ at the new time level plus known values of ζ and ζ_x. Note that the structure of any of the reduced forms of the generalized RBC (10) will be similar to those of either equations (11) or (12). Hence the finite element implementation for other specialized RBCs resulting from (10) follows from the preceding discussion.

* Note that outward travelling waves at $x = -L$ result in a change in sign for the ζ_x term in equation (19).

TEST CASES

In this section we discuss the test cases used to study the behaviour of the generalized RBCs relative to the Sommerfeld condition. The effectiveness of these RBCs is examined by comparing with solutions computed on a larger ('extended') grid where the propagating quantity does *not* feel the effect of the open boundary, i.e. the simulation is terminated before the boundary conditions influence the solution. For the telegraph and Klein–Gordon equations the generalized RBCs along with the Sommerfeld condition are studied for both their forced and unforced responses. In the forced case the RBC behaviour is investigated as $|\chi|$ in (9) is increased (τ/ω for the telegraph equation and $c^2\mu^2/\omega^2$ for the Klein–Gordon case) and as the open boundary is placed closer to the source of the wave motion. The parameters of interest are reported relative to a unit wavelength (λ) and a unit period (P) of the forcing (i.e. equation (25)). The spatial and temporal resolutions for all 1D calculations were maintained at 100 nodes/λ and $200\Delta t/P$ respectively, while the 2D example was computed on a grid with 40 nodes/λ and a time step size of $100\Delta t/P$.

Telegraph RBC

The forced case. The forced response case consists of the system initially at rest, $\zeta(x, t<0)=0$, with the centre node following a sinusoidal time history of

$$\zeta(0, t)=\sin(\omega t) \quad \text{for } t\geqslant 0. \tag{25}$$

To ensure that all transients have decayed in this experiment, the time-stepping scheme is

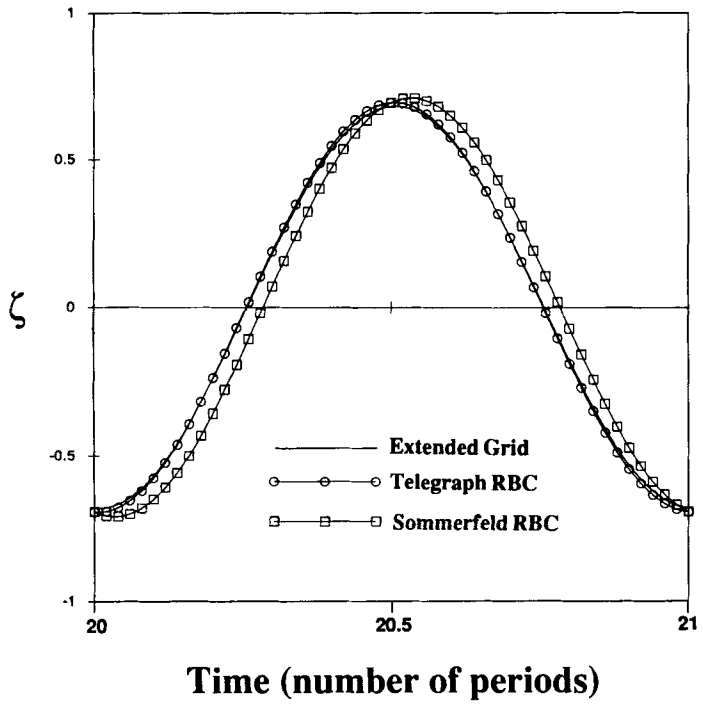

Figure 3. Calculated boundary value of the telegraph equation solution subject to various RBCs as a function of time once the dynamic steady state has been reached. Time is given in terms of number of periods into the simulation. The length of the grid is $\lambda/4$ and $\tau/\omega=0{\cdot}50$

advanced 20 periods prior to sampling the solution. If the distance between the location of the forcing and the open boundary is one wavelength and $\tau/\omega = 0{\cdot}50$, then the computed boundary values for the extended grid and telegraph RBC solutions are essentially indistinguishable—less than 1% difference—while the solution with the Sommerfeld RBC was within 3% of the overall peak (12% of the maximum boundary value) over one period. This level of accuracy was representative of the results obtained independent of τ/ω.

A more significant deterioration of the solution computed with the Sommerfeld RBC occurs as the length of the grid is reduced. Figures 3 and 4 show the solutions when the boundary is one-

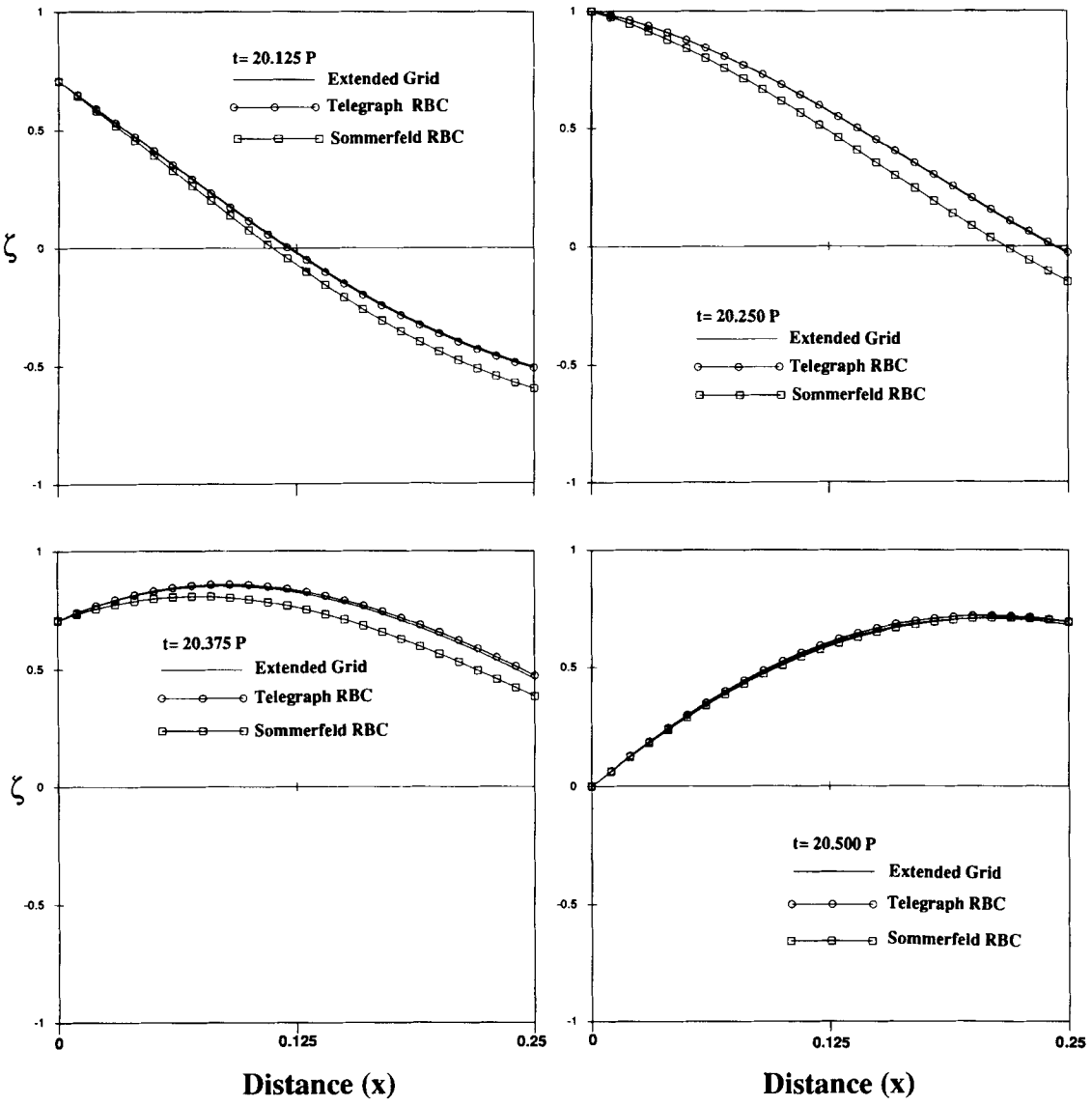

Figure 4. A time sequence of the spatial distribution of the telegraph solution subject to various RBCs. Times are 20·125, 20·25, 20·375 and 20·5 periods into the simulation. The length of the grid is $\lambda/4$ and $\tau/\omega = 0{\cdot}50$

quarter wavelength from the excitation and $\tau/\omega = 0{\cdot}50$. The inconsistency of the Sommerfeld RBC with the governing equation is apparent and the resulting errors are clear. The largest error in Figure 3 is 12% of the maximum value over one period for the Sommerfeld RBC (18% relative to the peak boundary value) compared to less than 1% for the telegraph RBC. When τ/ω is increased to 0·75, this error increases to 15% for the Sommerfeld condition (over 20% relative to the peak boundary value) but remains near 1% for the proposed telegraph RBC. A reduction in error (to below 10%) in the Sommerfeld condition case can be achieved either by reducing τ/ω or by extending the grid to a length greater than two wavelengths. In the first case, by reducing τ/ω, the problem is closer to the pure wave situation; in the second case, by increasing the length of the domain, the signal reaching the boundary is diminished, thus reducing the absolute size of the computed solution (and therefore the error).

The only troubling feature of the generalized RBC for the telegraph equation we have encountered thus far occurs in the case where the forcing contains a non-zero steady component. At a distance from the forcing corresponding to the position of the open boundary of the short grid, the extended grid solution shows the solution approaching the steady value imposed at the forcing end. This value is attained on a diffusive timescale. While the Sommerfeld condition solution on the short grid reaches the 'correct' boundary value—albeit on a timescale much too fast compared to the diffusive timescale—the telegraph RBC never reaches the correct value at the boundary.

The unforced case. The unforced response test case has as initial conditions the positive branch of a cosine function,

$$\zeta(x, t=0) = \cos(2\pi x/\lambda) \quad \text{for } |x| \leqslant \lambda/4, \tag{26a}$$

$$\zeta(x, t=0) = 0 \quad \text{elsewhere}, \tag{26b}$$

where λ corresponds to the wavelength of the forced response case. Since no forcing is applied, the initial disturbance is simply allowed to propagate through the grid.

Figure 5 shows the improvement obtained when the appropriate RBC is implemented for the telegraph equation. This is the same case as shown earlier in Figure 1. The steady state error found with the Sommerfeld RBC is removed and the time history of the solution is tracked more closely with the telegraph RBC (19). Quantitatively, the error induced by the Sommerfeld RBC is about 12% in the steady state while that of the telegraph RBC peaks around 3% and is smaller than the Sommerfeld RBC error at any point in time. Further, as the length of the grid is shortened to half a wavelength, the error with the telegraph RBC solution is approximately 5% while that of the Sommerfeld condition is closer to 20%. The level of error introduced by these boundary conditions is also dependent on τ: as τ increases (to 0·75), the errors in the telegraph RBC increase (to 6%–8%) but are less than the errors of the solution computed with the Sommerfeld RBC. In general, the solution with the telegraph RBC has been observed to decay faster than the extended grid solution would indicate, an effect which becomes more prominent with increasing τ.

Reflection coefficient analysis. Reflection coefficient analyses can also be used as a measure of the performance of RBCs.[12, 14] The reflection coefficient R can be found by assuming a solution to the telegraph equation of the form

$$\zeta = e^{j(\alpha x - \omega t)} + Re^{-j(\alpha x + \omega t)}, \tag{27}$$

where $\alpha = (\omega/c)\sqrt{(1 + j\tau/\omega)}$ from (7), and substituting this expression into the RBC under consideration. A smaller value of R corresponds to a smaller numerical reflection. Carrying out

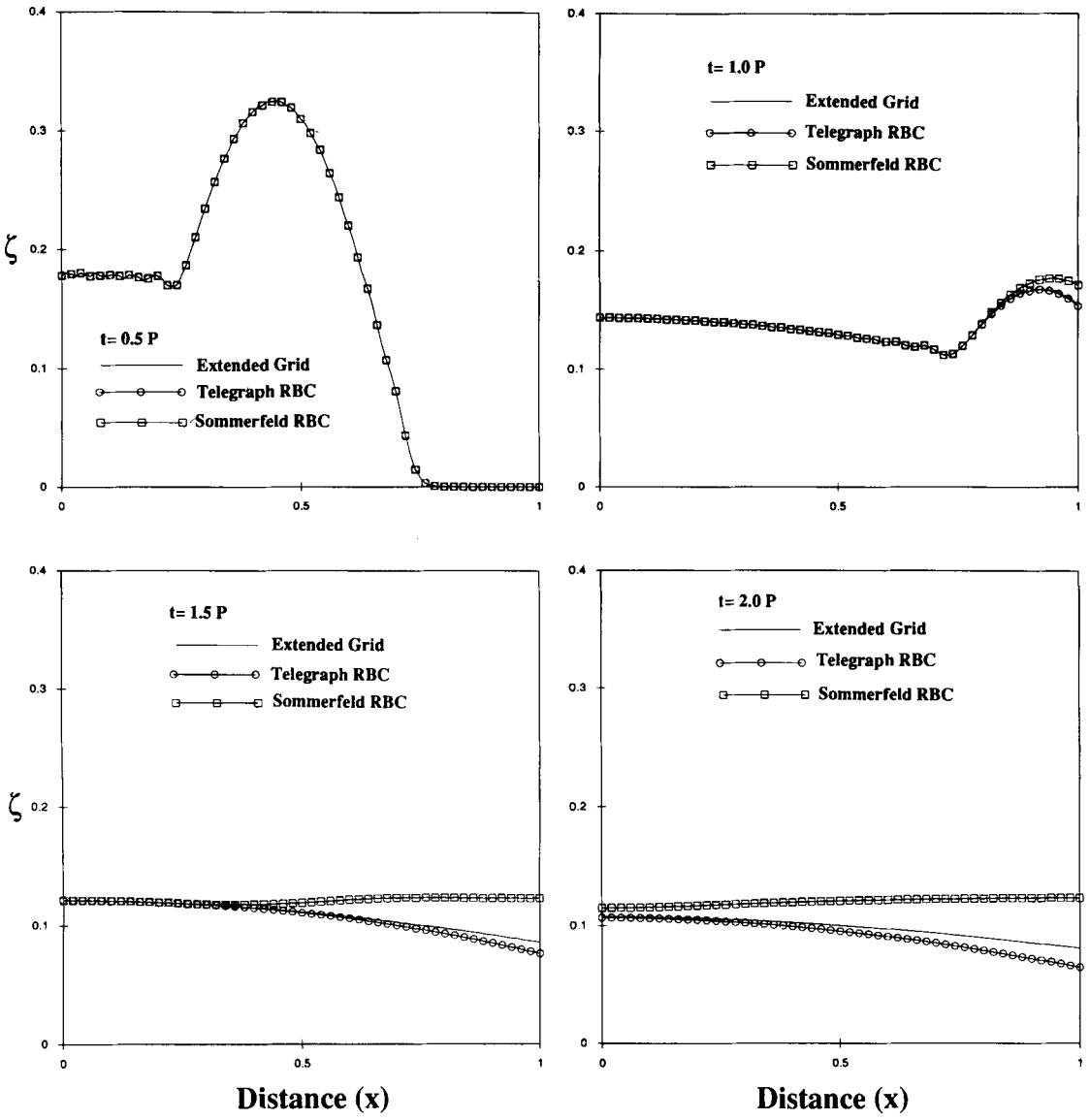

Figure 5. Same as Figure 1 except that the telegraph equation solution subject to the generalized RBC has been included. The length of the grid is λ, $\tau/\omega = 0{\cdot}5$ and the time instants occur 0·5, 1·0, 1·5 and 2·0 periods into the simulation

this procedure on equations (1a) and (19), and assuming normal incidence and a boundary at $x = 0$, results in the reflection coefficients

$$R_{\text{Som}} = \frac{\sqrt{(1+\mathrm{j}\tau/\omega)} - 1}{\sqrt{(1+\mathrm{j}\tau/\omega)} + 1}, \tag{28a}$$

$$R_{\text{tel}} = \frac{\sqrt{(1+\mathrm{j}\tau/\omega)} - 1 - \mathrm{j}\tau/2\omega}{\sqrt{(1+\mathrm{j}\tau/\omega)} + 1 + \mathrm{j}\tau/2\omega} \tag{28b}$$

when the telegraph equation governs and either (1a) or (19) is used as the accompanying RBC. Figure 6 shows the magnitude of these coefficients as a function of τ/ω, illustrating the improvement realized with the telegraph RBC (19).

Klein–Gordon RBC

The set-up for the forced and unforced cases is identical to those of the previous subsection for the telegraph RBC except that the governing equation is (3) and the proposed RBC is (12).

The forced case. Figure 7 shows the computed boundary value over the 21st period for a one-wavelength grid with $c^2\mu^2/\omega^2 = 0{\cdot}50$. As before, the solution on the extended grid and that subject to the Sommerfeld RBC are plotted for comparison. Figure 8 shows snapshots taken at four equally spaced time increments during the first half-period in the Figure 7. These plots are the same as those of Figure 2 where now the solution subject to the generalized RBC is shown.

The errors introduced by the RBCs are a function of space and time. The largest errors shown in Figures 7 and 8 for the Sommerfeld RBC approach 30% whereas the corresponding errors for the generalized RBC are less than 6%. These errors are also dependent on $c^2\mu^2/\omega^2$ and increase as this ratio increases. For example, with $c^2\mu^2/\omega^2 = 0{\cdot}75$ the solution can be off by as much as 100% at a point for the Sommerfeld RBC, while remaining within 12% when the Klein–Gordon RBC (12) is used. If $c^2\mu^2/\omega^2$ is reduced, the errors in both RBCs are likewise decreased. A series of numerical experiments have shown that for $c^2\mu^2/\omega^2 \leqslant 0{\cdot}25$ the Sommerfeld RBC behaves

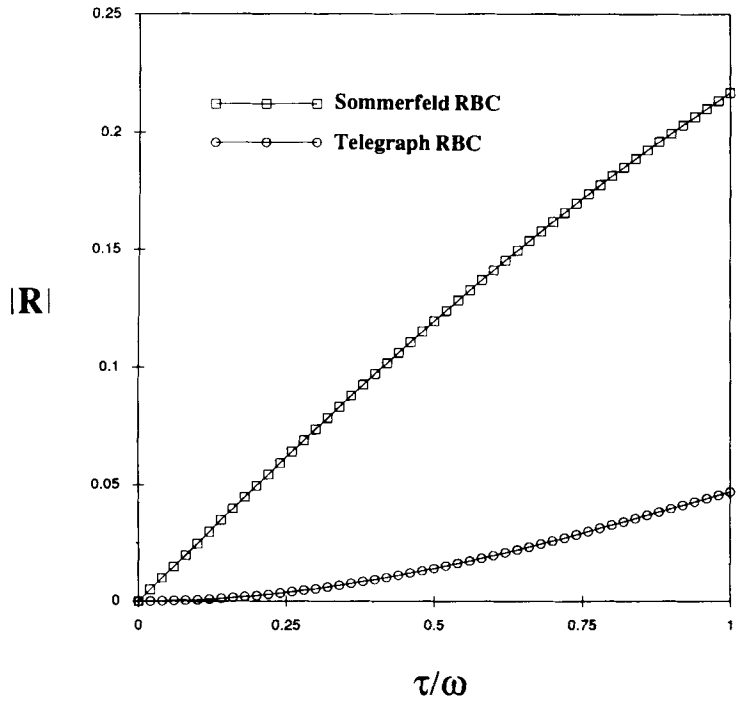

Figure 6. Magnitude of the reflection coefficient as a function of τ/ω when the telegraph equation governs and either the Sommerfeld or generalized RBC is invoked

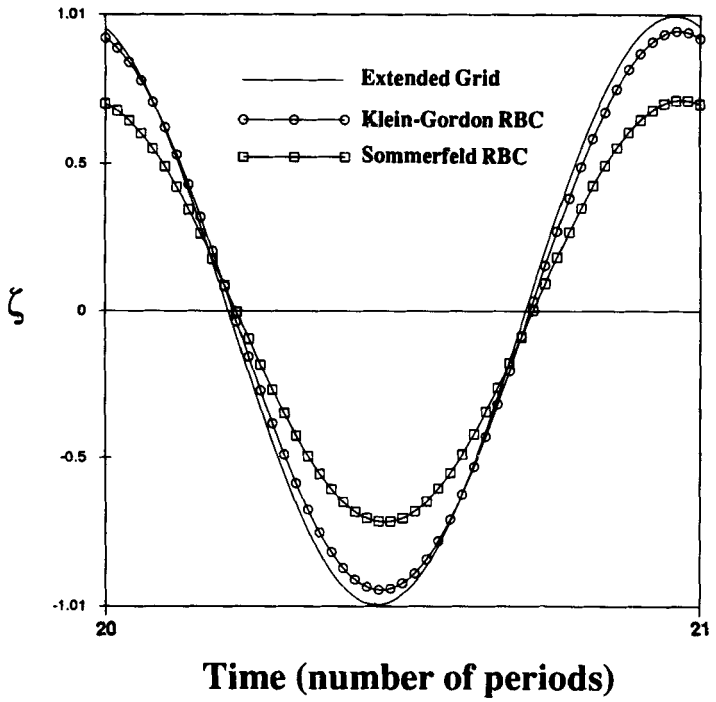

Figure 7. Computed boundary value for the Klein–Gordon equation solution subject to various RBCs as a function of time once the dynamic steady state has been reached. Time is given in terms of number of periods into the simulation. The length of the grid is λ and $c^2\mu^2/\omega^2 = 0{\cdot}50$

adequately, resulting in errors of the order of 10% or less. The solution with RBC (12) becomes almost indistinguishable ($\approx 2\%$) from the extended grid for such $c^2\mu^2/\omega^2$ ratios.

Unlike the telegraph equation where dissipation reduces the impact of reflections caused by RBCs as the length of the grid is increased, the errors remain of the same order for increasing grid length in this case. The shift in wavenumber[21] from ω/c to $\sqrt{[(\omega/c)^2 - \mu^2]}$ is not recognized by the Sommerfeld RBC; thus the incorrect phase and amplitude shifts observed in the solution for ζ.

The unforced case. A representative example of the unforced solutions subject to RBCs for the Klein–Gordon equation is shown in Figure 9. The length of the grid and coefficient values are identical to Figure 5. Four snapshots are shown, starting at a time when the initial disturbance (26a,b) has not yet reached the boundary and thus when all three solutions are identical. At later times the interaction with the RBCs takes effect and deviations begin to appear in the different solutions. The generalized RBC for the Klein–Gordon equation is consistently closer to the extended grid solution than the Sommerfeld RBC. This remains true for both increasing and decreasing values of μ and grid length. Variations of these parameters leads to a more severe deterioration of the solution with the Sommerfeld RBC (1a) than with the Klein–Gordon RBC (12). Errors introduced by the Sommerfeld RBC are typically of the order of 6% of the initial value (20%–30% of the peak value at a given time instant) compared to 2% (6%–10% of the peak at a given time) for the Klein–Gordon RBC.

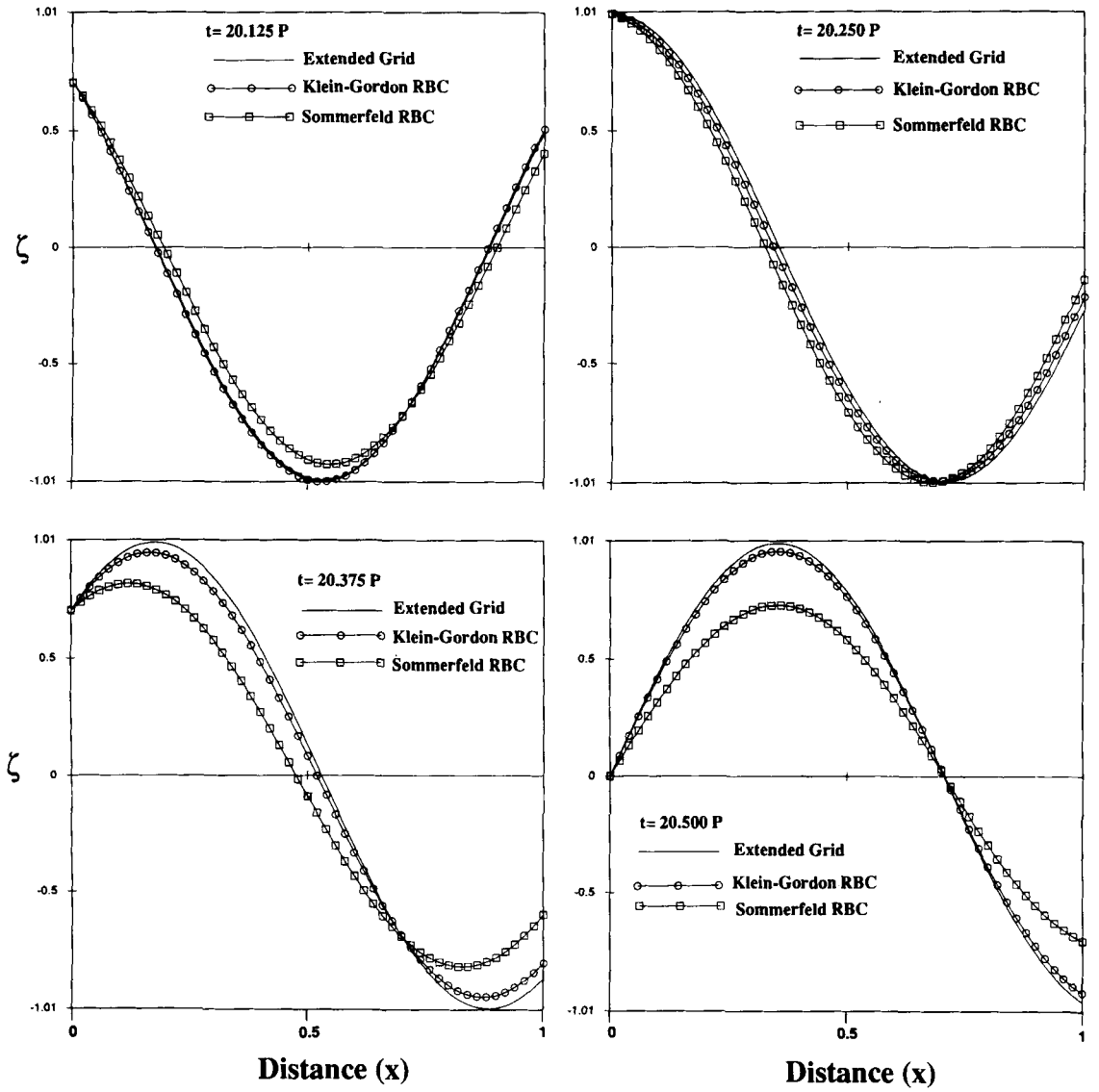

Figure 8. Same as Figure 2 except that the Klein–Gordon equation solution subject to the generalized RBC has been included. The length of the grid is λ, $c^2\mu^2/\omega^2 = 0{\cdot}50$ and the time instants occur 20·125, 20·25, 20·375 and 20·5 periods into the simulation

Reflection coefficient analysis. Reflection coefficient analysis for the Klein–Gordon case requires that a solution of the same form as (27) with $\alpha = (\omega/c)\sqrt{[1-(c\mu/\omega)^2]}$ be substituted into (1a) and (12). Solving for R results in reflection coefficients for normal incidence at a boundary located at $x = 0$ of

$$R_{\mathrm{Som}} = \frac{\sqrt{[1-(c\mu/\omega)^2]}-1}{\sqrt{[1-(c\mu/\omega)^2]}+1}, \tag{29a}$$

$$R_{\mathrm{KG}} = \frac{\sqrt{[1-(c\mu/\omega)^2]}+c^2\mu^2/2\omega^2-1}{\sqrt{[1-(c\mu/\omega)^2]}-c^2\mu^2/2\omega^2+1}. \tag{29b}$$

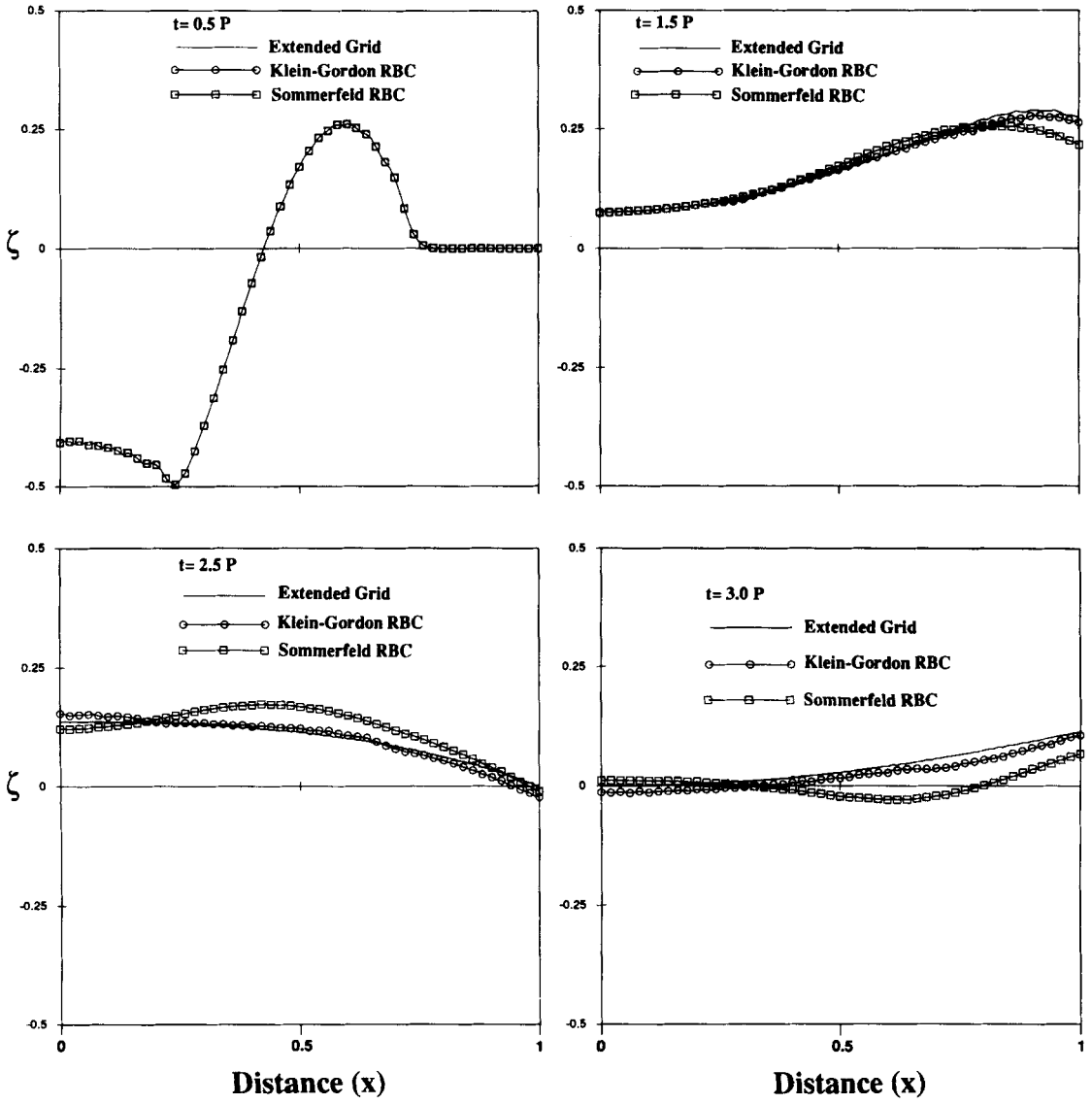

Figure 9. A time sequence of Klein–Gordon equation propagation of an initial disturbance subject to various RBCs. The length of the grid is λ, $c^2\mu^2/\omega^2 = 0{\cdot}50$ and the time instants occur 0·5, 1·5, 2·5 and 3·0 periods into the simulation

Figure 10 provides a plot of the magnitude of these coefficients as a function of $c^2\mu^2/\omega^2$. The improvement, particularly over the range $c^2\mu^2/\omega^2 \leqslant 0{\cdot}50$, obtained with the generalized RBC is evident.

A 2D example

As an example of implementing the generalized RBC in higher dimensions, a 2D calculation is included. While a systematic study comparable to that undertaken for the 1D case has not been

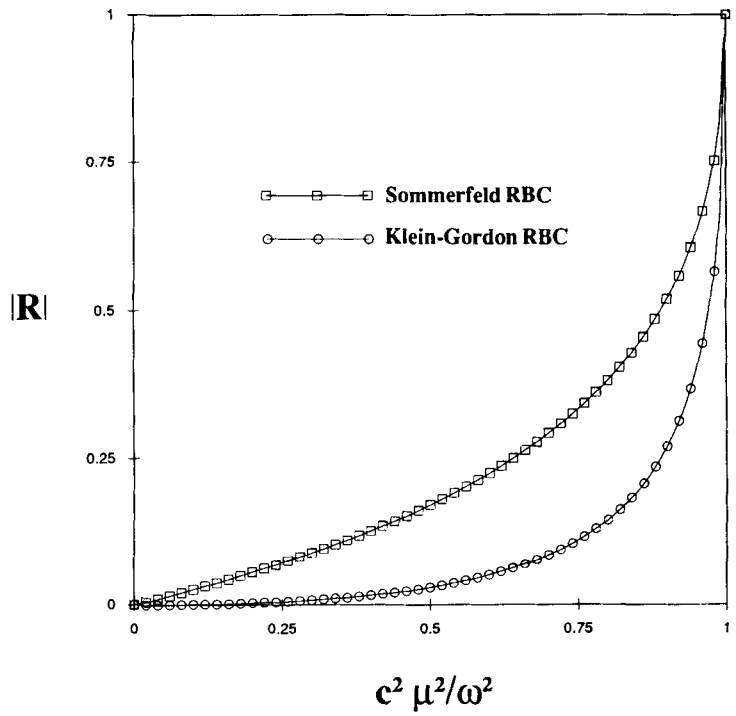

Figure 10. Magnitude of the reflection coefficient as a function of $c^2\mu^2/\omega^2$ when the Klein–Gordon equation governs and either the Sommerfeld or generalized RBC is invoked

completed, demonstration of feasibility is important with respect to finite elements given that this method is typically utilized for multidimensional problems. The 2D test case is a straightforward extension of the 1D telegraph case described above. The initial conditions are given by

$$\zeta(x, y, t=0) = \cos(\pi d/2d_0) \quad \text{for } d \leqslant d_0, \tag{30a}$$

$$\zeta(x, y, t=0) = 0 \quad \text{elsewhere,} \tag{30b}$$

where d_0 is the radius of a prescribed circle centred at (x_0, y_0) and d is the distance between a point of interest and the centre of the initial disturbance (x_0, y_0):

$$d = \sqrt{[(x-x_0)^2 + (y-y_0)^2]}. \tag{30c}$$

For the 2D wave equation the mound should collapse and a ring of fluid propagate radially outwards from its initial location. The 2D case shows a different behaviour than its 1D counterpart (Reference 21, pp. 843–847). While the solution for the 1D wave equation is always positive or zero (the initial displacement is also positive) and consists of two propagating pulses of identical shape and half the height, the solution of the 2D wave equation overshoots the 'zero' level and takes on negative values. Thus the pulse which spreads radially is followed by a wake which rebounds to the zero displacement level with time. Similarly, the solution for the 2D telegraph equation is a combination of the 2D wave equation solution and the diffusive effect discussed earlier.

Figure 11 shows a series of perspective plots for the telegraph RBC solution as a function of time. The wake trailing the initial wave front is evident and the disturbance propagates out of the

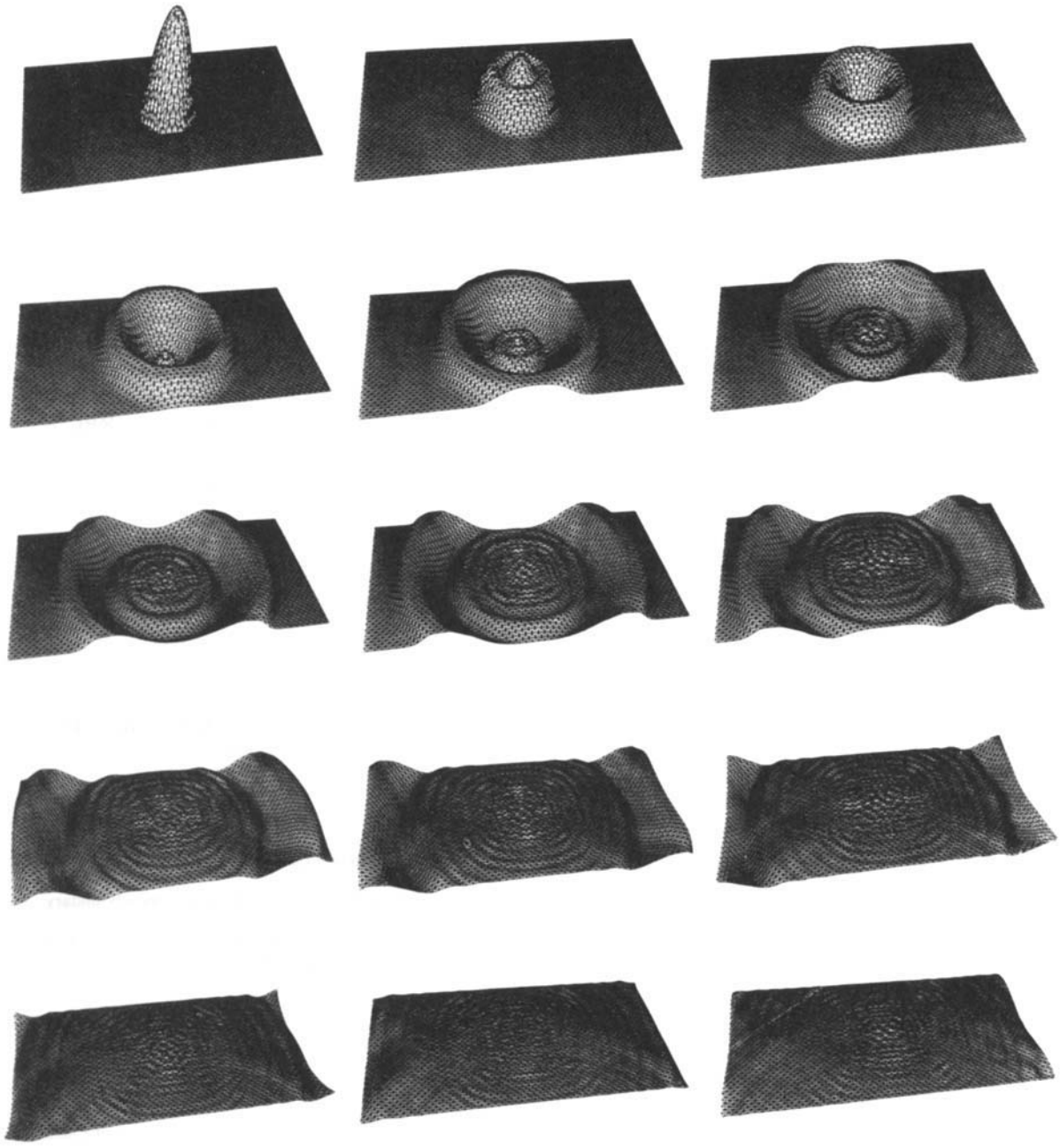

Figure 11. Perspective plot of a 2D telegraph equation solution subject to the generalized (telegraph) RBC for increasing time (upper left to lower right). The simulation shown was advanced a total of $700\Delta t$ with each plot representing a $50\Delta t$ increment. Relative to the half-wavelength cosine initial disturbance the grid is $1{\cdot}25\lambda$ long and $0{\cdot}625\lambda$ wide

computational domain without significant reflection. The plots in Figures 11 show that the solution is noisy. These errors are of the order of the grid spacing and result from insufficient resolution. The noisy portions of the solution are largely restricted to the centre of the grid where the most rapid changes occur (especially at early times). While these results are strictly preliminary, they are encouraging in that the generalized RBC has allowed the essential physics to be captured despite the use of a truncated grid.

CONCLUSIONS

A generalized radiation boundary condition for wave propagation is presented. Departures from the wave equation render the Sommerfeld RBC inconsistent with the governing equation and introduce non-negligible errors even in the simplest cases. To address this problem, a generalized form of the RBC is constructed by considering the dispersion relation for the general linear wave equation.

Two cases of the generalized RBC were studied by implementing finite element solutions for the telegraph and Klein–Gordon equations. Both forced and unforced problems were examined under simplified conditions. Compared to the Sommerfeld condition, the generalized RBC is desirable because it reduced the errors to only a few per cent when the generalized form of the wave equation governed the motions of interest. This level of improvement was observed in both the forced and unforced problems.

Only waves impinging at normal incidence on a boundary were studied in detail—corresponding to the 1D cases considered herein. Although the 2D results suggest that the main findings will generalize to higher dimensions, systematic studies in 2D and 3D remain to be done.

ACKNOWLEDGEMENTS

K.D.P. was supported by NIH grant CA45357. F.E.W. was supported by NSF grant CEE-8352226 and DOE grants DE-FG09-85ER60351 and DE-FG09-86ER60450.

REFERENCES

1. C. E. Pearson and D. F. Winter, 'On tidal motion in a stratified inlet with particular reference to boundary conditions', *J. Phys. Oceanogr.*, **14,** 1307–1314 (1984).
2. E. A. Martinsen and H. Engedahl, 'Implementation and testing of a lateral boundary scheme as an open boundary condition in a barotropic ocean model', *Coastal Eng.*, **11,** 603–627 (1987).
3. H. S. Chen, 'Infinite elements for combined diffraction and refraction', in T. J. Chung and G. R. Karr (eds), *Proc. VIIth Int. Conf. on Finite Element Methods in Flow Problems*, 3–7 April 1989, The University of Alabama in Huntsville Press, Huntsville, AL, 1989, pp. 653–658.
4. A. Sommerfeld, *Partial Differential Equations in Physics*, Academic Press, New York, 1949.
5. I. Orlanski, 'A simple boundary condition for unbounded hyperbolic flows', *J. Comput. Phys.*, **21,** 251–269 (1976).
6. B. Engquist and A. Majda, 'Absorbing boundary conditions for the numerical simulation of waves', *Math. Comput.*, **31,** 629–651 (1977).
7. A. C. Reynolds, 'Boundary conditions for the numerical solution of wave propagation problems', *Geophysics*, **6,** 1099–1110 (1978).
8. G. Mur, 'Absorbing boundary conditions for the finite-difference approximation of time-domain electromagnetic field equations', *IEEE Trans. Electromagn. Comput.*, **24,** 392–405 (1981).
9. W. H. Raymond and H. L. Kuo, 'A radiation boundary condition for multi-dimensional flows', *Q. J. R. Meteorol. Soc.*, **110,** 535–551 (1984).
10. G. K. Verboom and A. Slob, 'Weakly-reflective boundary conditions for two-dimensional shallow water flow problems', *Adv. Water Resources*, **7,** 192–197 (1984).
11. D. C. Chapman, 'Numerical treatment of cross-shelf open boundaries in a barotropic coastal ocean model', *J. Phys. Oceanogr.*, **15,** 1060–1075 (1985).

12. M. G. G. Foreman, 'An accuracy analysis of boundary conditions for the forced shallow water equations', *J. Comput. Phys.*, **64,** 334–367 (1986).
13. L. P. Røed and C. K. Cooper, 'Open boundary conditions in numerical ocean models', in J. J. O'Brien (ed.), *Advanced Physical Oceanographic Numerical Modelling*, D. Reidel, Dordrecht, 1986, pp. 411–436.
14. T. G. Moore, J. G. Blaschak, A. Taflove and G. A. Kriegsmann, 'Theory and application of radiation boundary operators', *IEEE Trans. Antennas Propag.*, **36,** 1797–1812 (1988).
15. J. G. Blaschak and G. A. Kriegsmann, 'A comparative study of absorbing boundary conditions', *J. Comput. Phys.*, **77,** 109–139 (1988).
16. R. P. Shaw, 'An outer boundary integral equation applied to transient wave scattering in an inhomogeneous medium', *J. Appl. Mech.*, **42,** 147–152 (1975).
17. R. W. Ziolkowski, N. K. Madsen and R. C. Carpenter, 'Three-dimensional computer modeling of electromagnetic fields: a global lookback lattice truncation scheme', *J. Comput. Phys.*, **50,** 360–408 (1983).
18. J. B. Keller and D. Givoli, 'Exact non-reflecting boundary conditions', *J. Comput. Phys.*, **82,** 172–192 (1989).
19. A. Bayliss and E. Turkel, 'Radiation boundary conditions for wave-like equations', *Commun. Pure Appl. Math.*, **23,** 707–725 (1980).
20. L. N. Trefethen and L. Halpern, 'Well-posedness of one-way wave equations and absorbing boundary conditions', *Math. Comput.*, **47,** 421–435 (1986).
21. P. M. Morse and H. Feshbach, *Methods of Theoretical Physics, Vol. I*, McGraw-Hill, New York, 1953.
22. D. R. Lynch and W. G. Gray, 'A wave equation model for finite element tidal computations', *Comput. Fluids*, **7,** 207–229 (1979).